Bioinformatics Profiling and Experimental Validation of 4 Differentially-Expressed LIM Genes in the Course of Colorectal-Adenoma-Carcinoma

Authors' Contribution:
Study Design A
Data Collection B
Statistical Analysis C
Data Interpretation D
Manuscript Preparation E
Literature Search F
Funds Collection G

ABEFG 1,2   **Ying He**
ACE 3   **Zongfu Pan**
B 1,2   **Qian Shi**
B 1,2   **Xilin Zhang**
D 1,2   **Weiyun Shen**
D 1,2   **Lixia Huo**
D 1,2   **Huihui Guo**
FG 1,2   **Chengwu Tang**
ACE 1,2   **Yuhang Ling**

1 Central Laboratory, The First Affiliated Hospital of Huzhou University, Huzhou, Zhejiang, PR China
2 Huzhou Key Laboratory of Translational Medicine, The First Affiliated Hospital of Huzhou University, Huzhou, Zhejiang, PR China
3 Department of Pharmacy, Zhejiang Provincial People's Hospital, People's Hospital of Hangzhou Medical College, Hangzhou, Zhejiang, PR China

Corresponding Authors: Yuhang Ling, e-mail: 52011@zjhu.edu.cn, Chengwu Tang, e-mail: tamgche@sina.com
Financial support: Zhejiang Natural Science Foundation (No. LQ20H160011), National Natural Science Foundation, People's Republic of China (No. 81970570), Zhejiang Medical and Health Science and Technology Project (No. 2019KY208, 2020KY310, 2022KY363, 2022RC264), and Huzhou Science and Technology Foundation Project (No. 2018GZ37, 2019GZ37)
Conflict of interest: None declared

Background: LIM domain proteins play crucial roles in tumors by interacting with diverse proteins. However, their roles in the course of colorectal mucosa-adenoma-carcinoma remain unclear. This study aimed to depict their dynamic expression profiles and elucidate their potential functions in this transition course.

Material/Methods: Differentially-expressed LIM proteins (DELGs) in paired adenomas, carcinomas, and mucosae were identified using the GEO dataset (GSE 117606) and validated by immunohistochemistry using our tissue microarray. Kaplan-Meier survival analysis, WGCNA, module-trait analysis, and KEGG enrichment were conducted. The correlation of DELGs expression levels with immune infiltration was assessed using the ESTIMATE package and TISCH database. The role of DELGs of interest was validated using cell proliferation, migration, and invasion assays.

Results: Four DELGs were identified – LMO3, FHL1, NEBL, and TGFB1I1 – all of which were of significance in prognosis. Module-trait correlation and KEGG enrichment revealed their involvement in cancer-related signaling. Immunohistochemistry showed gradual downregulation of LMO3 but upregulation of NEBL in the mucosa-adenoma-carcinoma sequence. The opposite expression patterns were observed for FHL1 and TGFB1I1 in tumor epithelium and mesenchyme. High expression levels of the DELGs were correlated with increased infiltration of NK, NKT, and macrophages, except for NEBL. Importantly, LMO3 inhibited proliferation, migration, and invasion of colon epithelial cells.

Conclusions: This study identified 4 differentially-expressed LIM genes – LMO3, FHL1, TGFB1I1, and NEBL – and revealed they were involved in the mucosa-adenoma-carcinoma sequence via regulating cancer-related pathways, influencing epigenetic field, or affecting immune infiltration. Our findings provide new insights into the roles of LIM proteins in the course of mucosa-adenoma-carcinoma.

Keywords: Colorectal Neoplasms • Computational Biology • Immunohistochemistry • LIM Domain Proteins

Full-text PDF: https://www.medscimonit.com/abstract/index/idArt/937081

📄 3701   ▦ —   📊 10   📚 41

Background

LIM domain proteins are a large family of cytoplasmic and nuclear proteins characterized by 2 or more tandem C-terminal LIM domains with or without N-terminal preLIM domains [1]. The LIM domain is a type of zinc finger that can interact with transcription factors and cytoskeleton-associated proteins, and thus play diverse roles in gene expression, cytoskeleton organization, immune function, and signal transduction [2,3]. Accumulating evidence shows LIM domain proteins are prominent molecules involved in onset and development of a wide variety of human cancers [4,5]. For instance, LMO, PDZ-LIM, zyxin, and LIMK were related to the malignant progression of colorectal, pancreatic, breast, and hematological cancers [2,6,7]. Of special interest, several members of LIM protein family are promising anti-cancer targets for drug development, such as LIMK [8,9]. Moreover, LIM domain genes are involved in innate and adaptive immunity by providing abundant zinc, whose levels are closely related to activity and homeostasis of immune cells [3]. Several recent studies have unveiled that expression levels of LIM domain proteins are correlated with tumor immune infiltration [10,11]. In colorectal cancer, an increasing number of LIM genes have been revealed to involve in cancer progression or suppression [12,13]. However, the dynamic profile and roles of LIM protein members during the adenoma-carcinoma sequence of colorectal tumors remains unclear.

The normal mucosa-adenoma-carcinoma sequence is a hallmark of colorectal carcinogenesis [14]. It is widely accepted that most colorectal cancers arise from polyps or adenoma, which is often the result of the APC inactivation. Subsequently, genetic mutations and cellular signal dysfunction correlated with cell apoptosis, survival, and proliferation are involved in the translation from adenoma to carcinoma [15]. Although multiple LIM proteins have been reported to promote or inhibit colorectal cancer progression, few studies have focused on the dynamic expression landscapes and roles of LIM proteins during the mucosa-adenoma-carcinoma sequence. To this end, we identified differentially-expressed LIM proteins and validated their expressions using paired samples of mucosa, adenoma, and carcinoma tissues. Furthermore, survival analysis, module-trait relationship and pathway enrichment, and immune infiltration analysis were conducted to understand the functions of the differentially-expressed LIM proteins. In vitro cell lines were used to validate the role of our LIM genes of interest in the adenoma-carcinoma course.

Material and Methods

Patient Samples

Retrospectively collected paired colorectal carcinoma, adenoma, and paracancerous normal mucosa tissues were included in this study. These tissues were resected from patients who underwent radical removal of colorectal cancers at the First People's Hospital of Huzhou between Jan 2018 and Oct 2019. Briefly, 51 carcinomas, 32 adenomas, and 53 normal mucosae were embedded and made into a tissue array. This study was approved by the Ethics Committee of the First People's Hospital of Huzhou (No. 2020KYLL002) and in line with the Declaration of Helsinki (as revised in 2013). All patients provided informed consent.

Cell Culture

Human colon adenocarcinoma cell lines HCT116 and RKO and normal colon epithelial cell line HCoEpiC were purchased from the Cell Bank of the Chinese Academy of Sciences (Shanghai, China). HCT116 was cultured with McCoy's 5A medium, while RKO and HCoEpiC were cultured in DMEM media supplemented with 10% fetal bovine serum (FBS).

Identification of Differentially-Expressed LIM Genes (DELGs)

The transcriptome data was downloaded from the dataset GSE117606 (Gene Expression Omnibus, https://www.ncbi.nlm.nih.gov/geo/) which included 69 adenomas, 74 carcinomas, and 65 mucosae from 70 patients. Differentially-expressed genes in normal mucosae, adenomas, and carcinomas were obtained using GEO2R (https://www.ncbi.nlm.nih.gov/geo/geo2r/) and the thresholds were chosen as False Discovery Rate (FDR) <0.05 and |log2(Fold change)| ≥1. Subsequently, identified genes then intersected with the LIM domain proteins [1]. The DELGs were presented in a heatmap by using the pheatmap package in R, and common DELGs among groups were analyzed in the Venn diagram using TBtools (Version 0.665). For shared DELGs in Venn diagram, their RNA expressions in mucosae, different subtypes of adenomas, and carcinomas were shown and the statistical significance were determined.

Survival Analysis

For common DELGs identified in Venn diagram, survival analysis was conducted using RNA expression and prognostic data of colorectal cancer in TCGA (The Cancer Genome Atlas, https://tcgadata.nci.nih. gov/tcga/). The optimal cut-offs for classifying patients into high and low gene expression groups were automatically calculated and survival curves were drawn by employing the survival package and survminer package in R3.5.1.

Immunohistochemistry

Immunohistochemistry results for the common DELGs identified in Venn diagram were attained from the Human Protein Atlas database (https://www.proteinatlas.org). Additionally,

immunohistochemistry validation was done using sections (4-μm) of our tissue microarray. In brief, those sections received microwave antigen retrieval after routine dewaxing and hydration, followed by endogenous peroxidase enzyme and antigen blocking using 5% goat serum. Anti-LMO3 (Bioss, Cat#bs-5938R, 1: 25, Beijing, China), anti-FHL1 (Bioss, Cat#bs-9525R, 1: 50, Beijing, China), anti-NEBL (Bioss, Cat#bs-9468R, 1: 100, Beijing, China), and anti-TGFB1I1 (Proteintech, Cat#10565-1-AP, 1: 50, Wuhan, China) primary antibodies were incubated with sections at 4°C overnight, and rabbit IgG (Beyotime, Cat#A7016, 1: 100, Shanghai, China) was used for the negative control. On the next day, biotin-labeled secondary antibodies, streptavidin-HRP, DAB, and hematoxylin were sequentially incubated with the tissue sections according to the instructions of the Rabbit&Mouse HRP Kit (CwbioTech., Taizhou, China). Finally, digital immunohistochemical images were scanned on a TMA scanner (3D Histech, Hungary) and analyzed using the H-scores system. H-score=1×(% cells 1+)+2×(% cells 2+)+3×(% cells 3+).

Weighted Correlation Network Analysis (WGCNA)

The co-expression network for the common DELGs was established using the WGCNA package in R3.5.1. The sample clustering was conducted to exclude outlier samples, followed by scale independence and mean connectivity analysis to determine the soft threshold. A cluster dendrogram was depicted using default settings to generate different gene modules, and the eigengene adjacency heatmap was drawn.

Module-Trait Analysis

Patient age, sex, pathological subtype, and expression profiles of the 4 common DELGs were selected as clinical traits. Then, we conducted module-trait correlation analysis and the |correlation index| >0.5 and $p<0.05$ was considered significant.

Kyoto Encyclopedia of Genes and Genomes (KEGG) Enrichment Analysis

The modules which were the most negatively or positively correlated with tissue pathology or DELGs were chosen for KEGG pathway enrichment analysis. The enrichment was performed using ClusterProfiler package in R. Significant pathways were identified when the FDR <0.05. The top 10 pathways and frequency of related genes were visualized by ggplot2 package.

Immune Infiltration Analysis

ImmuneScore, StromalScore, and ESTIMATEScore among high- and low-expression groups (classified by the median value) of the 4 DELGs were determined using the estimate package in R3.5.1. Furthermore, the Spearman's correlation analysis was conducted to compare the detailed infiltrated immune cells

and the expression abundances of the 4 DELGs by using data from the TISCH database (http://tisch.comp-genomics.org).

Plasmid Transfection and Cell Proliferation, Migration, and Invasion Assay

Human LMO3 CDS was cloned into pcDNA3.4 vector to construct pcDNA3.4-LMO3-3×Flag. HCoEpiC, HCT116, or RKO cells were seeded into 6-cm dishes at 50% confluence and cultured overnight. pcDNA3.4-LMO3-3×Flag or empty vector was transfected into cells using Ez-Trans reagent (Life iLAB, Shanghai, China) according to the manufacturer's instructions. Twenty-four hours after transfection, the cells were digested and seeded into E-16 plates for cell proliferation assay, or CIM-16 plates and Transwell chambers (Corning, USA) for cell migration and invasion assays. For invasion assay, the CIM-16 plates and Transwell chambers were pre-coated with diluted matrigel (Corning, Dilution 1: 10, USA). Cell index was recorded using the Real-time Cell Analysis xCELLigence® system (ACEA Biosciences, USA). For Transwell assays, migrated and invaded cells were fixed with 4% PFA, washed with phosphate-buffered saline (PBS), and then stained with 1% crystal violet solution (w/v) and observed under microscopy.

Western Blots

Forty-eight hours after plasmid transfection, cells were harvested and lysed by RIPA strong lysis buffer (Beyotime, Shanghai, China) supplemented with protease inhibitor on ice for 30 min. The supernatants were obtained by centrifugation (13 000 rpm, 10 min) and then submitted to SDS-PAGE electrophoresis separation, followed by transferring protein samples into PVDF membranes. The membranes were subjected to 5% BSA blocking for 1 h and then anti-LMO3 primary antibody incubation (Bioss, Cat#bs-5938R, 1: 1000, Beijing, China) at 4°C overnight. After incubation with HRP-conjugated secondary antibody (Beyotime, Cat#A0208, 1: 1000, Shanghai, China) for 1 h, the immunoblots were visualized using BeyoECL Plus Kit (Beyotime, China) on Tanon Gel Imaging System (Tanon 4600, China).

Statistical Analysis

Data are presented as mean±SD unless special description and statistical analysis was conducted in Graphpad Prism 8 and R3.5.1 software. The unpaired t test was used to compare the 2 groups. $P<0.05$ was considered statistically significant.

Results

DELGs Along the Mucosa-Adenoma-Carcinoma Sequence

For paired mucosa, adenoma, and carcinoma specimens from 70 patients in GSE117606, the relative mRNA expressions
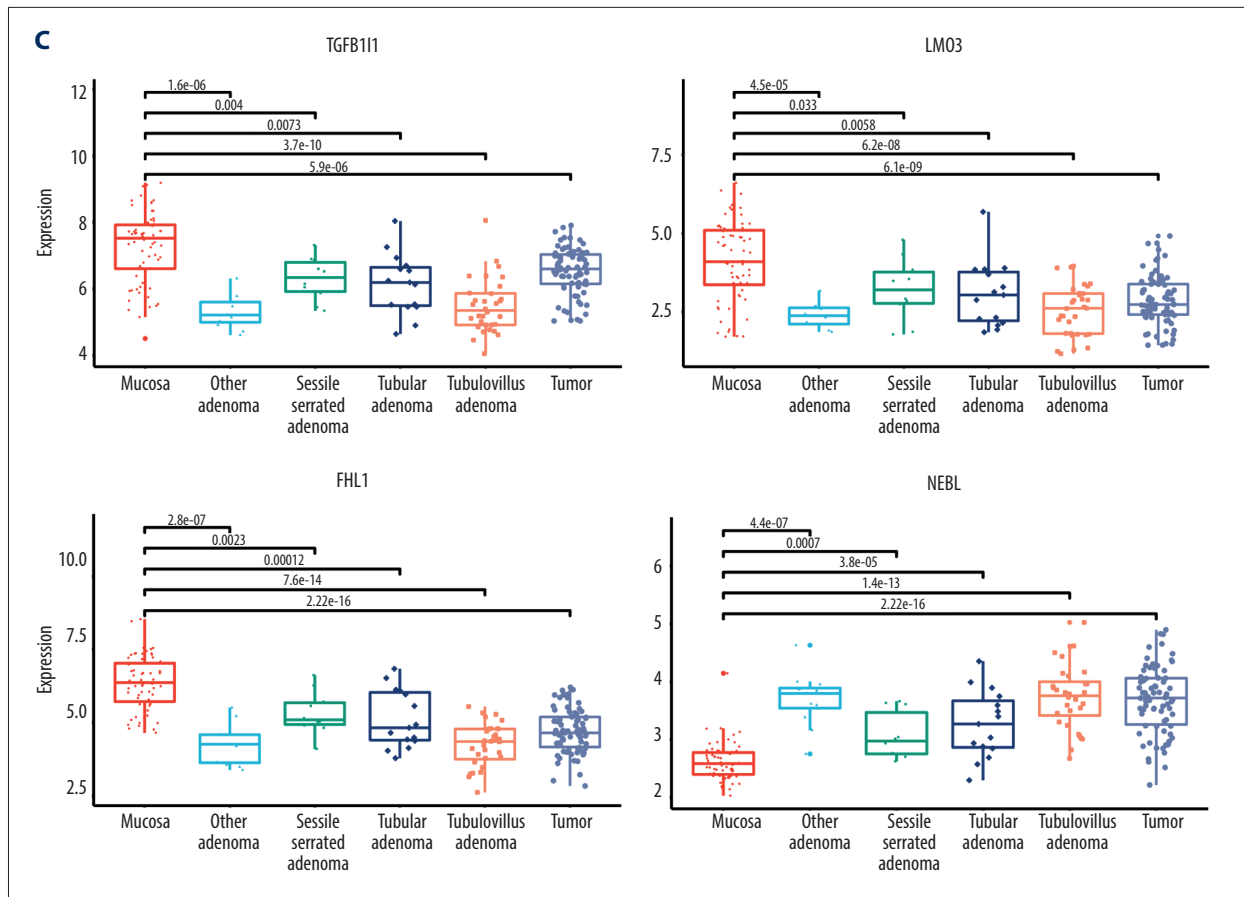
A

B
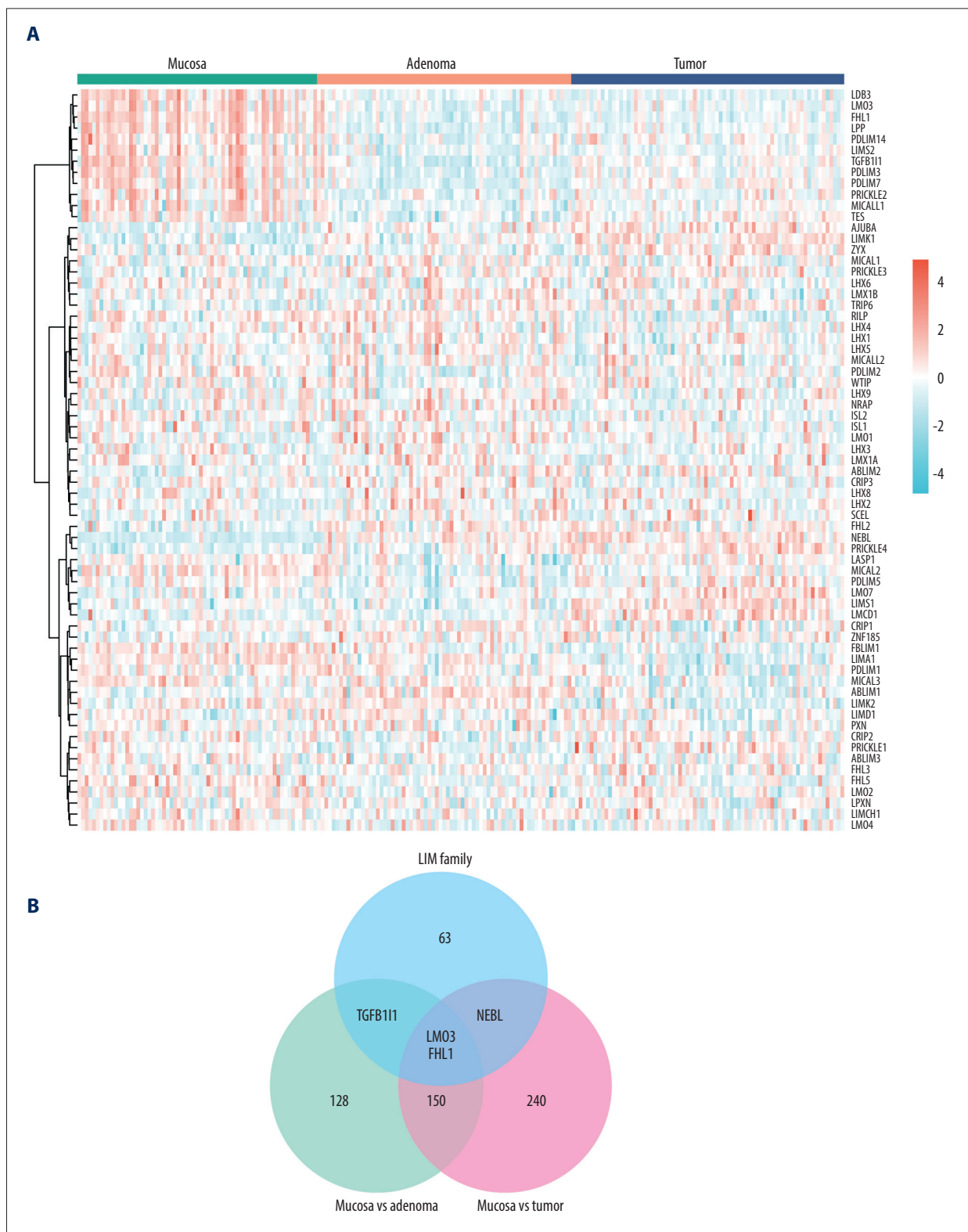
Figure 1. Identification of differentially-expressed LIM genes (DELGs) in the mucosa-adenoma-carcinoma course. (**A**) Expression levels of LIM family genes in paired mucosa, adenoma, and carcinoma samples from the GSE117606 dataset were drawn in a heatmap. (**B**) Common DELGs from adenoma vs mucosa, and tumor vs mucosa are presented in a Venn diagram. (**C**) Expression of DELGs in mucosa, different types of polyps, and tumors (R, version 3.5.1; TBtools, version0.665).

of LIM proteins are depicted in the heatmap (**Figure 1A**). As shown in the Venn diagram, 4 differentially-expressed LIM genes (DELGs) – LMO3, FHL1, NEBL, and TGFB1I1 – were identified by intersecting the LIM gene list with differentially-expressed genes between adenoma vs mucosa, and carcinoma vs mucosa (**Figure 1B**). Compared with normal mucosae, LMO3, TGFB1I1, and FHL1 were significantly downregulated in multiple types of adenomas and tumors, while NEBL was markedly upregulated (**Figure 1C**). Importantly, LMO3 and FHL1 were the most common downregulated DELGs between adenoma vs mucosa and carcinoma vs mucosa.

Survival Analysis and Expression Validation of DELGs

We evaluated the prognostic value of the 4 DELGs using survival data from TCGA database. High expressions of LMO3, TGFB1I1, and FHL1 were correlated with poor survival, while high NEBL expression predicted long survival time (**Figure 2A**). Although the prognostic values of LMO3, TGFB1I1, and FHL1 were incompatible with their RNA expression patterns, this

might be due to the complex components of the tumors, which consist of tumor cells, stromal cells, immune cells, and others. Actually, the gene expression pattern in tumors is not necessarily in line with its prognostic role, although it is common to hypothesize the consistency. For example, Ogino et al revealed Cyclin D1 was overexpressed in colorectal cancers, yet high Cyclin D1 predicted a better prognosis [16]. The tissue heterogeneity and range of tumor molecular features could be underlying reasons.
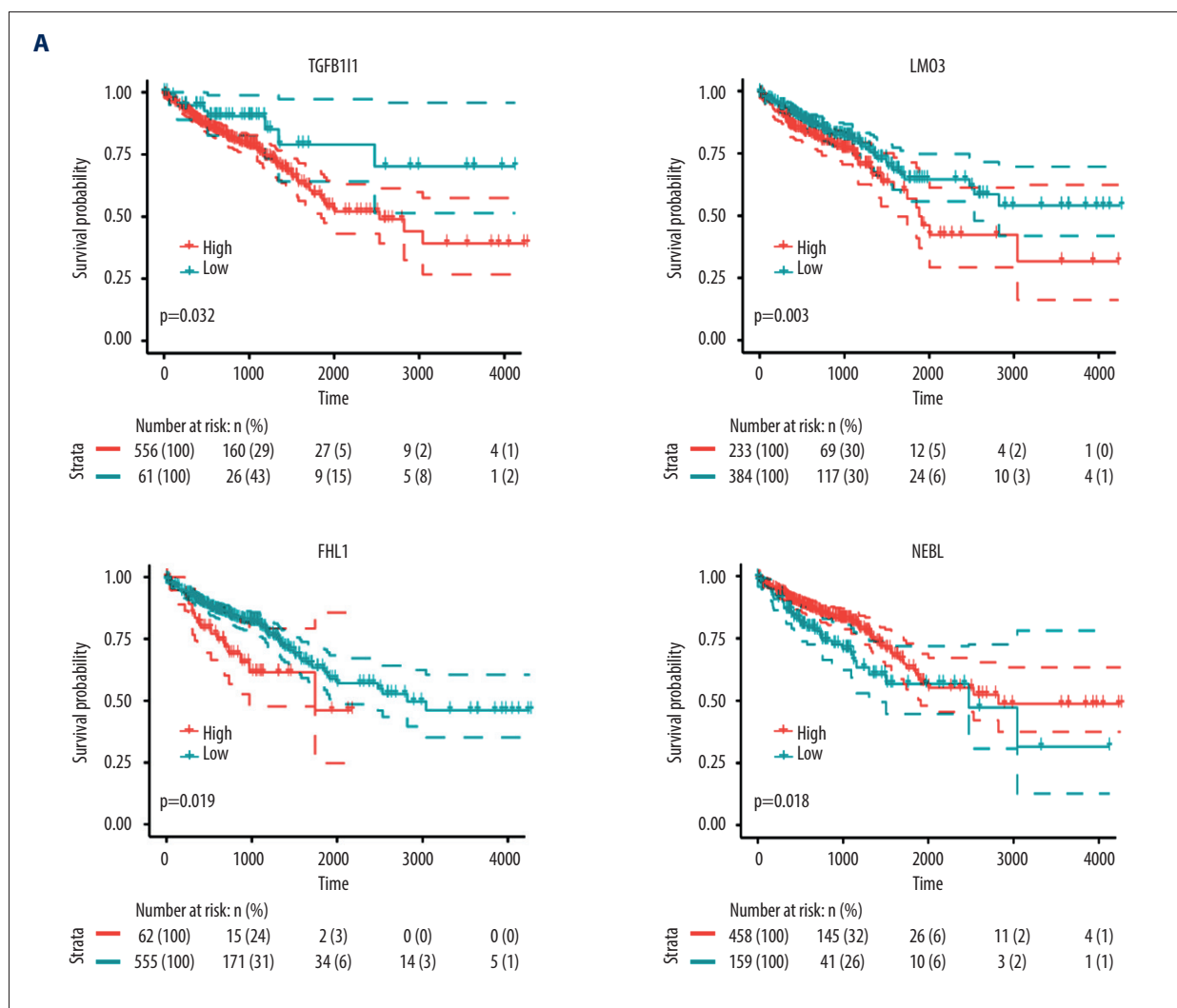
Next, the expression profiles of the 4 DELGs were validated using immunohistochemical results from the Human Protein Atlas database (**Figure 2B**) and our tissue microarray (53 mucosae, 32 adenomas and 51 carcinomas included). For negative control slides, rabbit IgG instead of primary antibodies was incubated and the results showed negative staining (**Supplementary Figure 1**). The database data showed that FHL1 and TGFB1I1 were downregulated in COAD and READ tissues when compared with unpaired normal mucosae.

In our microarray analysis, the expression intensity and percentages were assessed using H-scores and samples included in the statistical analysis are indicated in **Figure 3** (samples without target tissues on the slides were excluded). Of note, FHL1 and TGFB1I1 expressions were enhanced in epithelial tumor cells when compared with paired mucosae or adenomas in our microarray, while these 2 proteins were downregulated in the tumor mesenchyme (**Figure 3A, 3B**). In both the database and our microarray, NEBL expression was gradually increased in the mucosa-adenoma-carcinoma sequence in the epithelium. LMO3 was downregulated in tumors compared with adenoma and mucosa, which was in line with the mRNA expression profiles in GSE117606 (**Figure 1C**).

WGCNA and module-trait analysis

In the sample clustering, no outlier mucosa, adenoma, or carcinoma samples in the GSE117606 were found; thus, all samples were subjected to subsequent analysis (**Figure 4A**). By scale independence and mean connectivity analysis, the best β soft threshold value was automatically determined as 8 (**Figure 4A**). Then, a total of 11 gene modules were obtained and are presented using different colors (**Figure 4B**). The eigengene adjacency heatmap between those modules is shown in **Figure 4C**, indicating MEblack and MEgreen are clustered, and MEred, MEbrown, MEmagenta, and MEpurple are adjacent. Next, the 4 DELGs, patient age, gender, and tissue malignancy grades represented by pathological subtypes were chosen as the traits, and their relationships with those 11 modules were analyzed and are presented in **Figure 4D**. Notably, the expression levels of all the 4 DELGs were closely related to MEyellow module (NEBL, cor=-0.62, *p*=7e-24; FHL1, cor=0.91, *P*=3e-81; LMO3, cor=0.84, *P*=6e-57; TGFb1I1, cor=0.87, *P*=1e-65). NEBL also showed a strong correlation with MEblue (cor=-0.65, *P*=3e-26) and MEgreen (cor=0.85, *P*=8e-60) modules, while LMO3 and FHL1 were weakly associated with those 2 modules. Additionally, MEgreen (cor=0.75, *P*=3e-38), MEblack (cor=0.61, *P*=1e-22), and MEyellow (cor=0.78, *P*=2e-44) modules

This work is licensed under Creative Common Attribution-
NonCommercial-NoDerivatives 4.0 International (CC BY-NC-ND 4.0)

e937081-6

Indexed in: [Current Contents/Clinical Medicine] [SCI Expanded] [ISI Alerting System]
[ISI Journals Master List] [Index Medicus/MEDLINE] [EMBASE/Excerpta Medica]
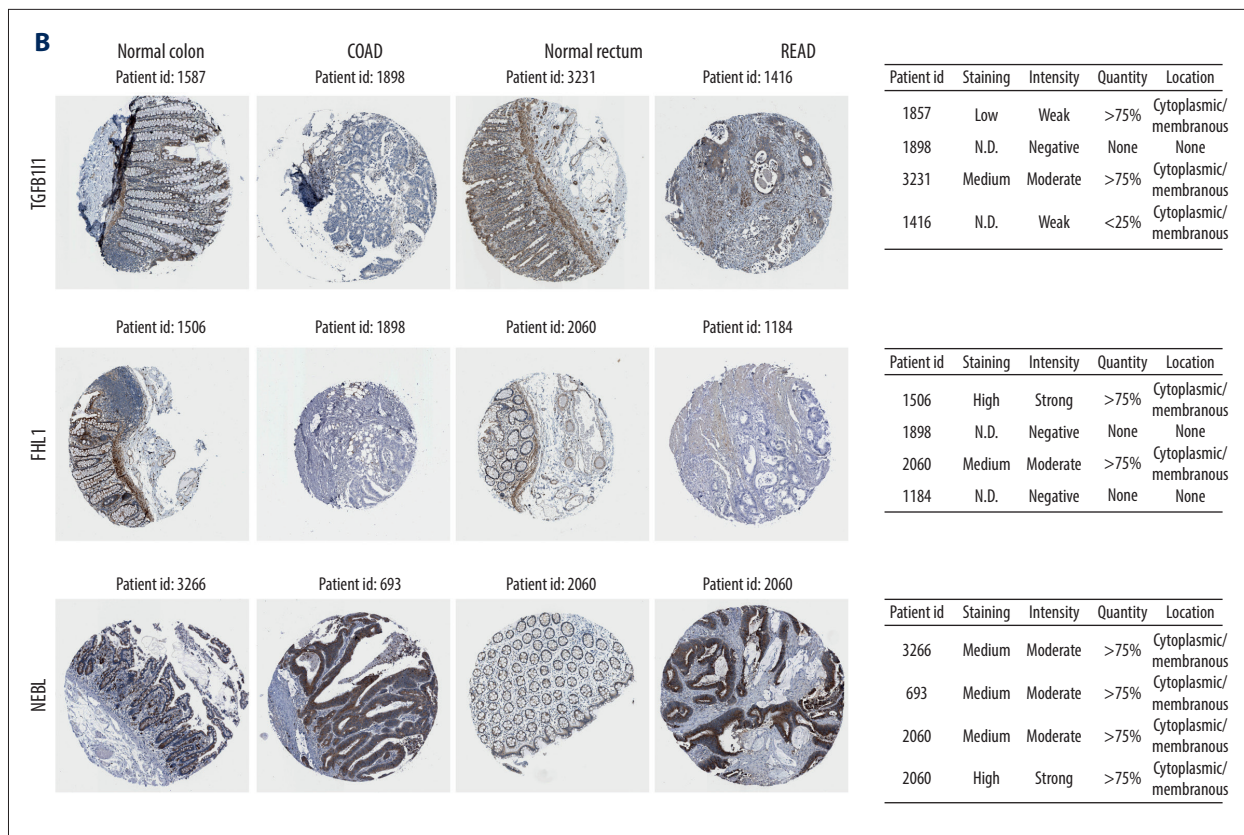[Chemical Abstracts/CAS]

Figure 2. Prognostic significance of the DELGs and their protein expressions in the Human Protein Atlas database. (**A**) The Kaplan-Meier survival curves of the 4 DELGs in colorectal cancers are depicted. Patients were classified into "High" and "Low" groups based on the gene expression levels, and the median value was chosen as the cut-off. (**B**) The protein expression and cellular locations of the 4 DELGs were validated by immunohistochemical images from the Human Protein Atlas database (R, version 3.5.1).

were significantly correlated with tissue pathological subtypes, which were closely associated with tissue malignancy grades.

KEGG Enrichment for Trait-Related Modules

Next, KEGG enrichment analysis was conducted for the most related modules of the 4 DELGs, including MEyellow, MEblue, and MEgreen modules. Based on the FDR, the top 10 significantly enriched pathway terms are presented in **Figure 5A**. MEgreen was enriched with "Wnt signaling pathway" and "Cell cycle", both of which were vital pathways in colorectal cancer development [17,18], suggesting that LMO3, NEBL, FHL1, and TGFB1I1 are involved in regulation of Wnt and cell cycle pathways. MEblue was significantly enriched in "Chemical carcinogenesis" and multiple metabolism pathways such as "Sulfur metabolism" and "Drug metabolism", suggesting the related NEBL and FHL1 might play a role in chemical metabolism regulation. For MEyellow module, "Focal adhesion", "ECM-receptor interaction", and "Gap junction" were listed in the top 10 enriched pathways, which was consistent with the well-known roles of LIM proteins [2]. **Figure 5B** presents all the enriched

pathways and the frequency of enriched genes. Of special interest, MYL9 and AKT3 in MEyellow module appeared with high frequency, which were reported to be associated with cell migration and tumorigenesis in several cancers [19,20]. Drug metabolism genes like UGT1A6 and UGT1A8 were expressed 7 times higher in the MEblue module, indicating the 4 DELGs and tissue malignancy degree may be associated with functions of metabolizing enzymes. Additionally, MYC and CCND2, which are 2 well-known oncogenic genes [21,22], both were expressed 2 times higher in MEblue modules.

Correlation with immune infiltration

To assess the relationships between components in the tumor microenvironment (TME) and the expression abundances of the 4 DELGs, ESTIMATE analysis was performed. ImmuneScores in **Figure 6A** revealed the positive relationships of LMO3, FHL1, and TGFB1I1 expression levels with the proportions of immune cells in TME. Similarly, high StromalScores and ESTIMATEScores (**Supplementary Figure 2**) were also significantly associated with high expression abundances of LMO3, FHL1, and TGFB1I1.
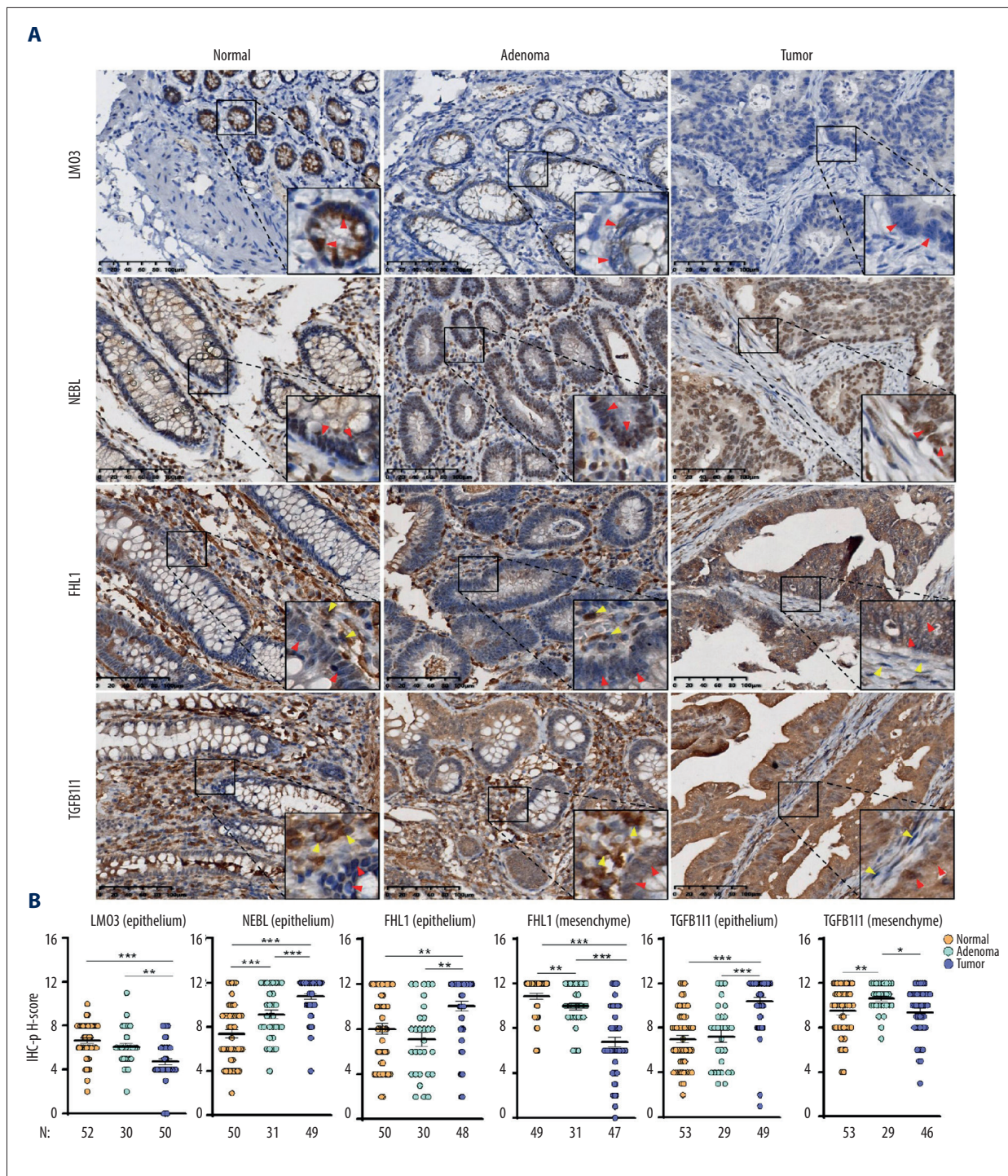
Figure 3. Immunohistochemical validation of the 4 DELGs using mucosa, adenoma, and carcinoma tissues from colorectal cancer patients. (**A**) Immunohistochemical images. Red and yellow triangles indicate positive expression in the epithelium and mesenchyme, respectively. (**B**) The expression intensity and positive percentages of the 4 DELGs are represented using H-scores. Data are shown as the mean±SEM (Graphpad, version 8.0.2).

By contrast, we observed that there was an obvious increase of ImmuneScore and ESTIMATEScore accompanying the decline of NEBL expression. Given that the 4 DELGs could influence the ratios of stromal and immune cells, we further investigated their correlations with specific immune components. The lollipop chart shows that LMO3 expression was positively related to tumor-infiltrating mast cells, NK cells, and macrophages (**Figure 6B**, Cor >0.4, *P*<0.01). FHL1 and TGFB1I1 expression levels both showed strong positive correlations with multiple infiltrating immune cells, including mast, macrophages, NK,

Treg, Th1, CD4, and Tfh cells (**Figure 6B**, Cor >0.4, *P*<0.01). In line with the result of ESTIMATE analysis, NEBL expression was negatively associated with the infiltrating levels of the majority of immune components in TME, such as CD56dim NK, CD8 TEM, and MDSC cells (**Figure 6B**, Cor <-0.3, *P*<0.01). A possible explanation for the link between immune infiltration and LIMs is that LIM genes could alter cytokine secretion of tumor cells by interacting with downstream targets. It is well-established that cytokines play an important role in regulating immune function. For example, LIM domain protein LASP1 was
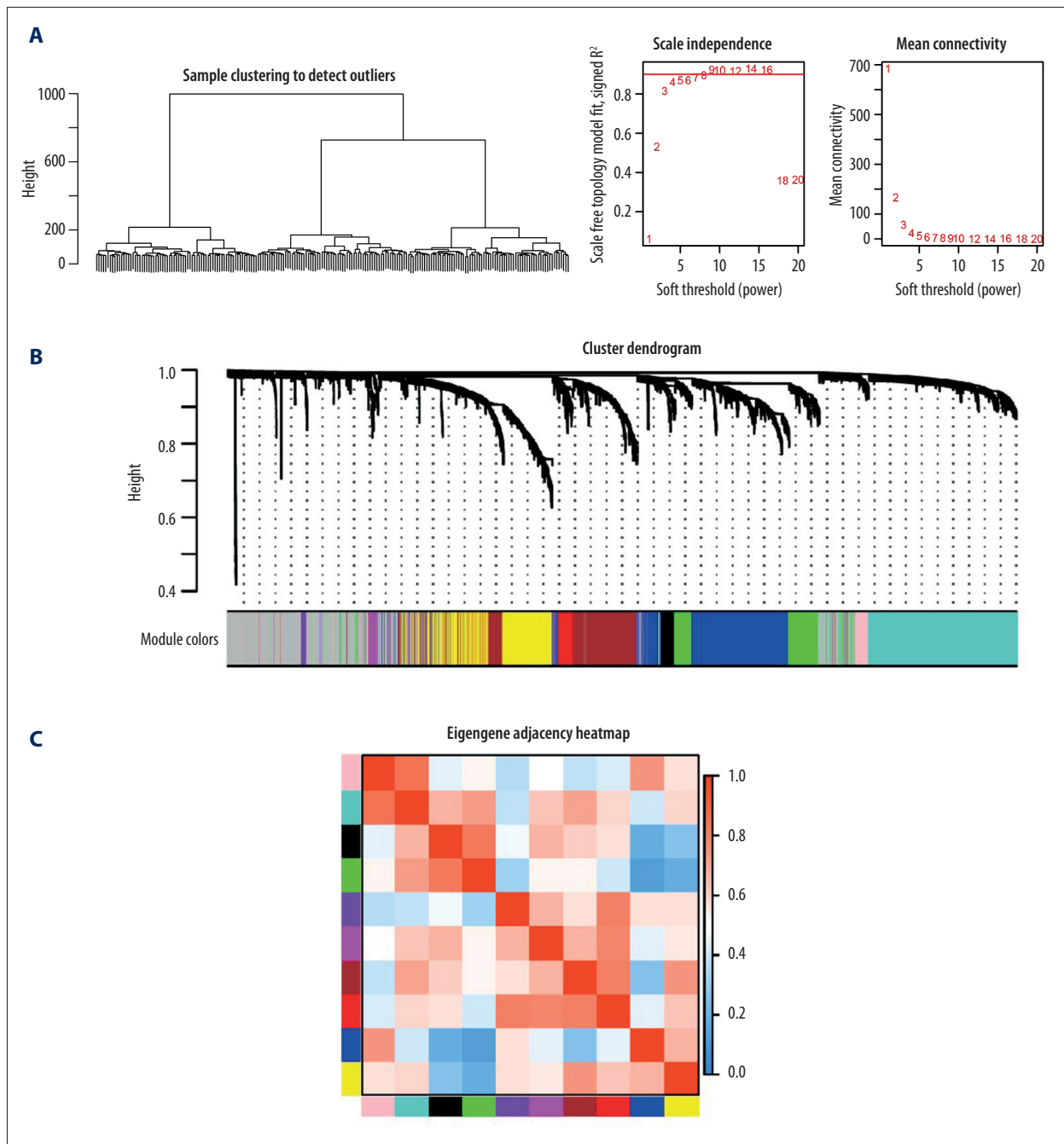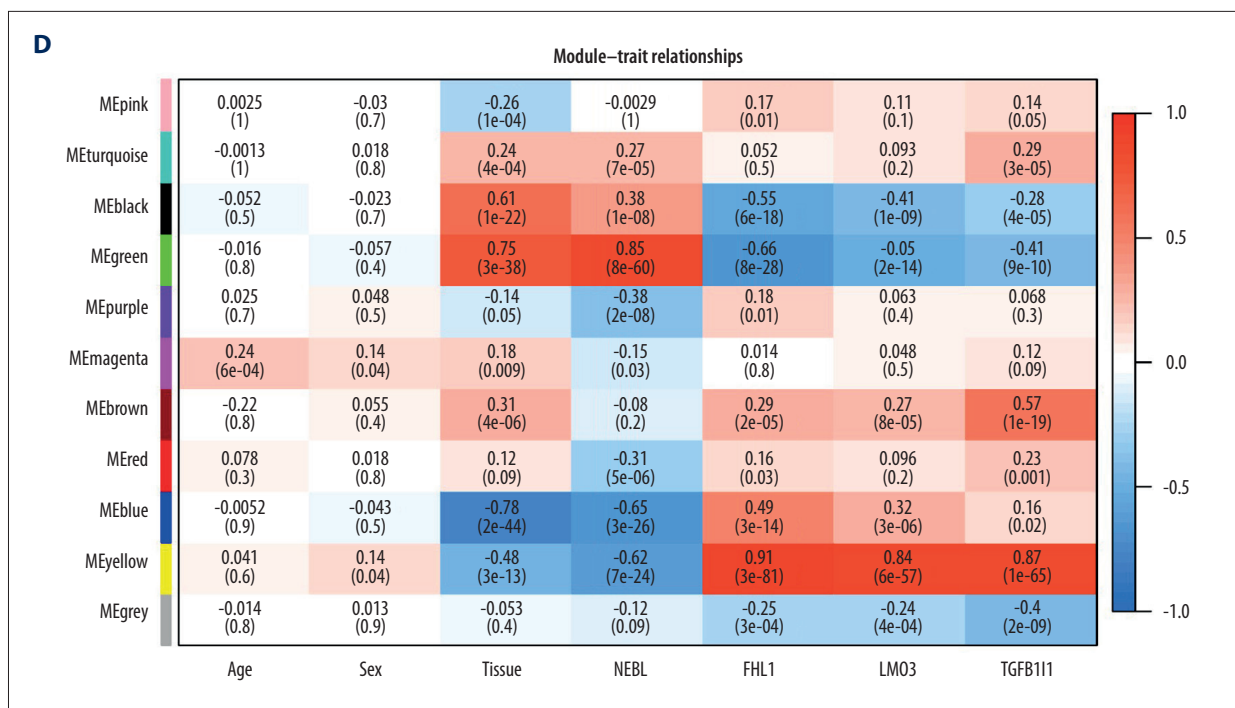
Figure 4. WGCNA and Module-trait correlation analysis. (**A**) Sample clustering analysis was performed to exclude outlier samples from GSE117606 and the best β soft threshold was determined depending on scale-free topology and mean connectivity analysis. (**B**) A hierarchical clustering of the eigengene modules. (**C**)The adjacency between the eigengene modules is presented in the heatmap. (**D**) Correlations between the traits (the 4 DELGs, patient age, gender, and pathological subtypes) and the eigengene modules were analyzed and shown in the heatmap (R, version 3.5.1).

reported to bind to CXCR4 and influence the cytokine release in chronic myeloid leukemia cells, which in turn affected immune function of T lymphocytes and NK cells [23]. Additionally, LIMs also participate in immune-related signaling, such as IL-15 and IL-9 signals [13].

LMO3 Inhibited Colorectal Cell Proliferation, Migration, and Invasion

Since the role of LMO3 in colorectal cancer is unknown, so we further assessed the protective role of LMO3 in the mucosa-adenoma-carcinoma sequence. The cell overexpression was validated by western blot (**Supplementary Figure 3**). Cell proliferation and migration were observed using the Real-time Cell Analysis xCELLigence® system and Transwell assay. As presented in **Figure 7A**, LMO3 overexpression reduced the proliferation and migration cell indices of both colon cancer cells (HCT116 and RKO) and normal colonic epithelial cells (HCoEpiC). Migrated cells stained by crystal violet further demonstrated that LMO3 overexpression weakened the migration potentials of HCT116 and HCoEpiC cells (**Figure 7B**). LMO3 overexpression could also inhibit cell invasion of HCT116 and RKO cells (**Figure 7B**), indicating LMO3 acts as a tumor-suppressor in the course of colorectal mucosa-adenoma-carcinoma progression.

Discussion

LIM proteins often consist of appropriately spaced repeats of LIM domains and act as prominent biosensors in cells by mediating protein–protein interaction [1,9,24]. Although multiple LIM proteins were reported to be involved in cancers, the dynamic changes of LIM proteins during the colorectal mucosa-adenoma-carcinoma sequence remain obscure. In this study, we depicted their expression profiles and found 4 DELGs, namely LMO3, FHL1, TGB1I1, and NEBL. Next, prognostic significance, module-trait relationship, KEGG enrichment, and in vitro experiments were conducted to comprehensively understand the role of these proteins in the mucosa-adenoma-carcinoma transition.

LMO3 belongs to the LIM-only family and has been reported as an oncoprotein in several cancers, including glioma [25], lung cancer [26], and hepatocellular carcinoma [27], whereas its activity in the colorectal sequence remains poorly characterized. In the present study, we observed a gradual decrease of LMO3 expression in the mucosa-adenoma-carcinoma sequence at mRNA and protein levels (**Figures 1, 3**). Survival analysis revealed that high LMO3 predicted poor patient outcomes, which was consistent with its negative correlation with glioma and neuroblastoma prognoses [25,28]. Interestingly, our cell experiments
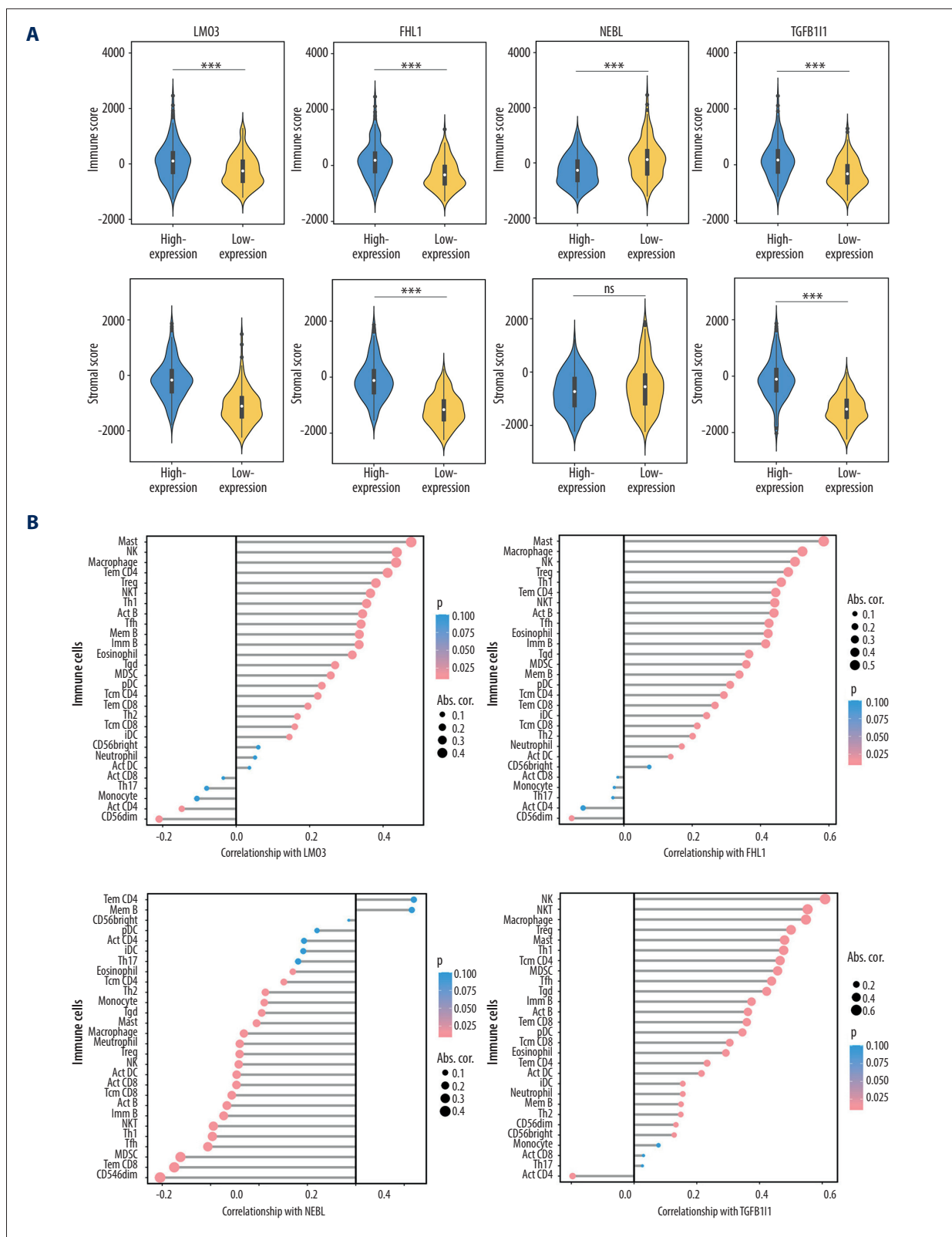
Figure 5. KEGG pathway enrichment for significant modules. (**A**) Top 10 enriched pathways are listed for the significantly correlated modules (MEgreen, MEyellow, and MEblue) of the tissue pathological subtypes and the 4 DELGs in the module-trait correlation analysis. (**B**) All significantly enriched pathways and the frequency of correlated genes in MEgreen, MEyellow, and MEblue modules (R, version 3.5.1).

Figure 6. The 4 DELGs were correlated with immune infiltration. (**A**) Significantly different ImmunoScores and StromalScores in high- and low-expression groups of the 4 DELGs assessed by ESTIMATE package in R3.5.1. (**B**) Lollipop charts shows the correlations of 28 types of immune cells with expression levels of the 4 DELGs (R, version 3.5.1).

showed that LMO3 could suppress carcinogenesis through inhibiting cell proliferation, migration, and invasion, which is opposite to its oncogenic role in some cancers. In consideration of its diverse functions as a docking site of protein complexes [29], it is possible that it binds with distinct proteins in different cancers and exerts contrasting downstream activities. Mechanistically, our module-trait analysis suggests LMO3 might be involved in Wnt and cell cycle signaling in tumors, and future experiments are needed to elucidate the molecular mechanisms through which LMO3 plays a cancer-suppressive role.

FHL1, which is located in chromosome Xq26.3, was previously shown to be inactivated in various tumors, such as gastric [30], lung [31], and colon cancer [32]. Actually, our study found that FHL1 was silenced in the adenoma stage compared with that in the normal mucosa, which was far before the adenoma-carcinoma transition. Consistently, FHL1 methylation and silencing was observed in precancerous lesions of gastric cancer, such as

Helicobacter pylori-infected lesions and non-cancerous colonic mucosae [32]. Thus, FHL1 inactivation was expected to contribute to the formation of an epigenetic field for cancerization, which was crucial in the mucosa-adenoma-carcinoma sequence. Meanwhile, the immunostaining demonstrated the inactivation of FHL1 was more obvious in the mesenchyme than that in the epithelium, suggesting FHL1 in stromal cells also is important in the sequence. In line with this, our immune infiltration analysis and a recent study both revealed that FHL1 levels were closely associated with immune infiltration of T cells, NK cells, and macrophages [13]. Thus, the role of FHL1 in TME is warrants further studies, although the tumor-suppressive activities of FHL1 in colorectal tumor cells are relatively well-studied.

NEBL encodes 3 isoforms – Nebulette, LASP2, and LIM-nebulette – and was primarily found to regulate cell adhesion and actin filament [33]. The role of NEBL in tumors is controversial and both oncogenic and tumor-suppressive functions have been described
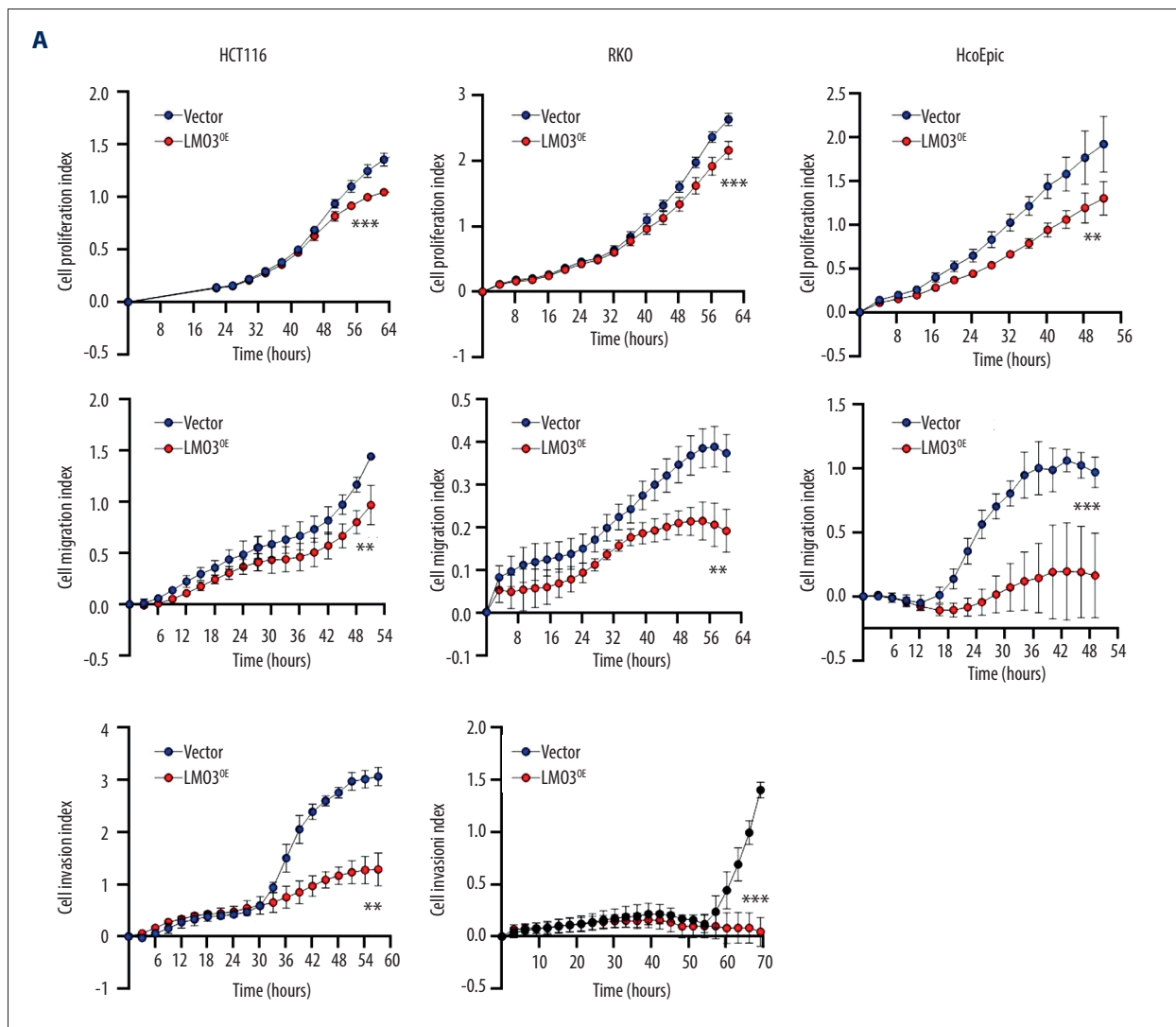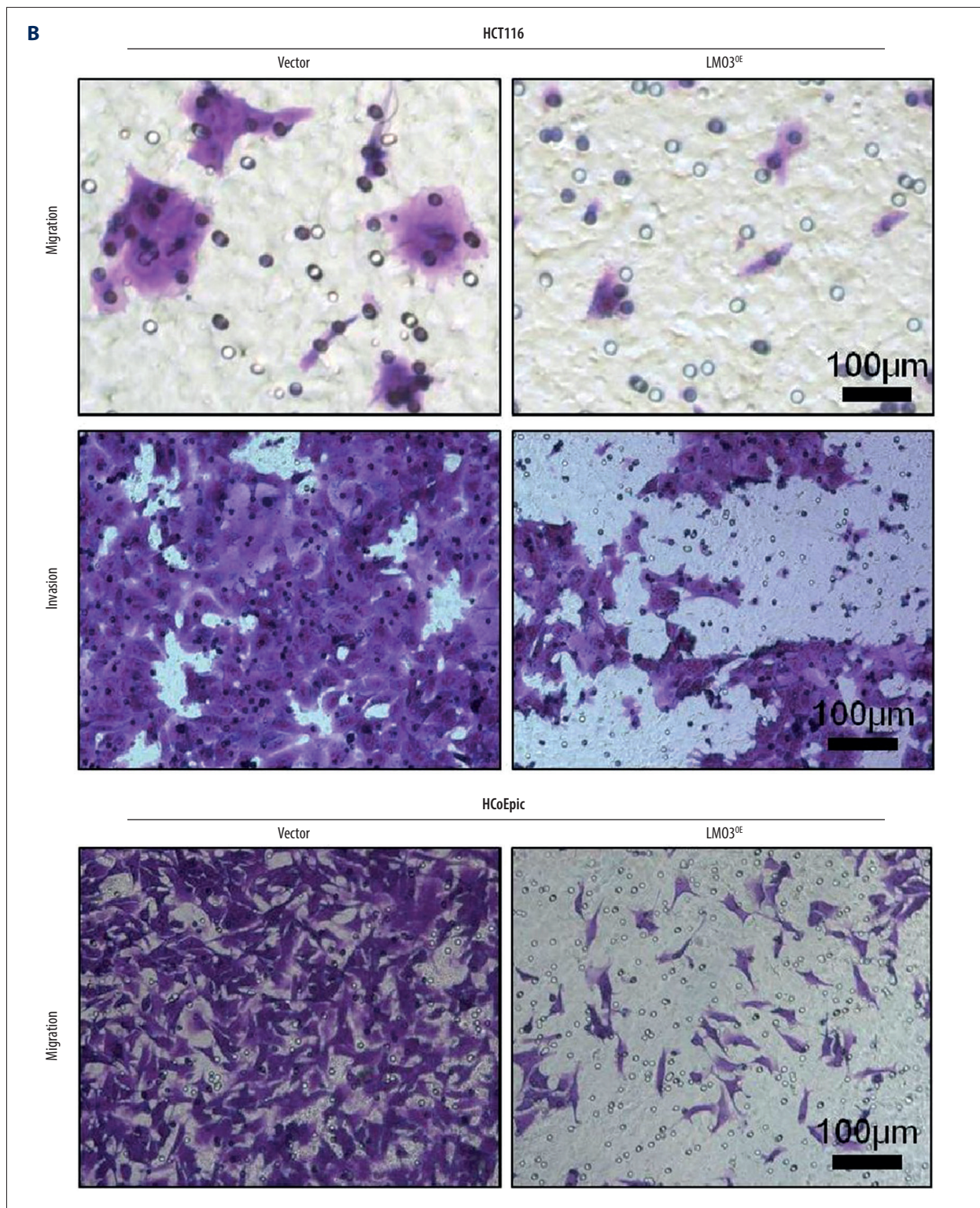
Figure 7. LMO3 overexpression inhibited colorectal cell proliferation, migration, and invasion. (**A**) Cell proliferation and migration indices of normal colon epithelial cells (HCoEpiC) and colon cancer cells (HCT116 and RKO) monitored by Real-time Cell Analysis system. For each group, at least 3 biological replicates were included in the analysis. (**B**) Migrated or invaded cells in Transwell chambers stained by 1% (w/v) crystal violet solution. For each group, at least 3 biological replicates were included in the analysis (Graphpad, version 8.0.2).

[34,35]. For instance, it contributed to liver cancer progression by activating the MAPK/ERK pathway [36] but inhibited cervical cancer by suppressing TGF-β-induced epithelial-mesenchymal transition [35]. Even in colorectal cancer, conflicting expression profiles and roles were reported [33,37]. In the present study, we found the gradually increased expression of NEBL in the mucosa-adenoma-carcinoma sequence for the first time. Moreover, NEBL presented opposite correlations with MEgreen and MEblue modules as compared with that of LMO3, FHL1, or TGFB1I1, suggesting distinct functions of NEBL in Wnt and cell cycle pathways. In immune infiltration analysis, we observed a strong correlation of NEBL with CD56dim NK and CD8+ T cells, which are both vital components in immunotherapy [38], indicating that NEBL is involved in immune regulation. This result was supported by the findings from a highly homologous protein of NEBL – LASP1 – which influences cancer relapse by regulating chemokines [23].

TGFB1I1 (also known as Hic-5) encodes a focal adhesion scaffold protein and has previously been demonstrated to contribute to cancer-associated fibroblast-governed tumor extracellular matrix (ECM) remodeling [39,40]. As the interplay between immune cells and cancer ECM is crucial in stromal remodeling [41], it is important to note the correlation between immune infiltration and TGFB1I1 expression. Our analysis showed that TGFB1I1 expression was positively related to macrophages and NK cells. Macrophages play a major role in upregulating synthesis and assembly of collagens, especially collagen types VI, and inducing ECM deposition [41]. Interestingly, TGFB1I1 also presented strong a correlation with ECM-receptor pathway-related genes, including COL6A1/2 (collagen types VI). Thus, it is reasonable to hypothesize the involvement of TGFB1I1 in the crosstalk between infiltrated immune cells and ECM deposition.

However, there are also limitations of our study. Only 1 dataset was included in the identification of differentially-expressed LIM genes and the sample size was limited. Future experiments using data from different cohorts and datasets and further molecular and in vivo validations are needed to clarify the roles of the 4 DELGs in adenoma-carcinoma transition.

Conclusions

In summary, this study is the first to perform dynamic expression profiling of LIM family genes along the normal mucosa-adenoma-carcinoma progression and identified 4 differentially-expressed LIM genes: LMO3, FHL1, TGFB1I1, and NEBL. NEBL expression indicated favorable prognosis, while the other 3 genes were correlated with poor survival. Additionally, high LMO3, TGFB1I1, and FHL1 were associated with increased immune infiltration, but NEBL abundance suggested less infiltration of the majority of immune cells. Of note, we revealed LMO3, whose role in colorectal tumors was unknown, acts as a tumor-suppressor in colorectal tumorigenesis. Future experimental studies are needed to reveal the detailed molecular mechanisms of their functionality, and more attention should be paid to the interplay between these 4 LIM proteins and tumor microenvironment components, including immune cells.

Department and Institution Where Work Was Done

The work was done in the First Affiliated Hospital of Huzhou University, Huzhou Key Laboratory of Translational Medicine, Huzhou, Zhejiang, PR China.

Declaration of Figures' Authenticity

All figures submitted have been created by the authors, who confirm that the images are original with no duplication and have not been previously published in whole or in part.
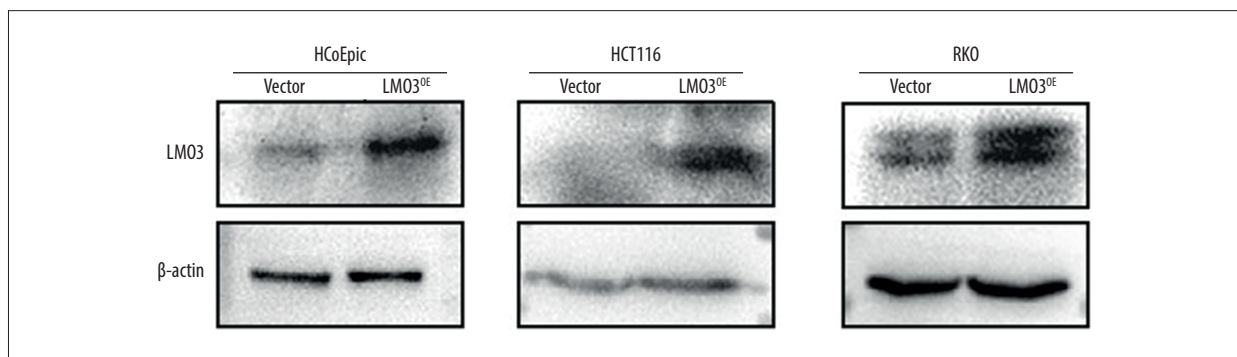
Supplementary Material
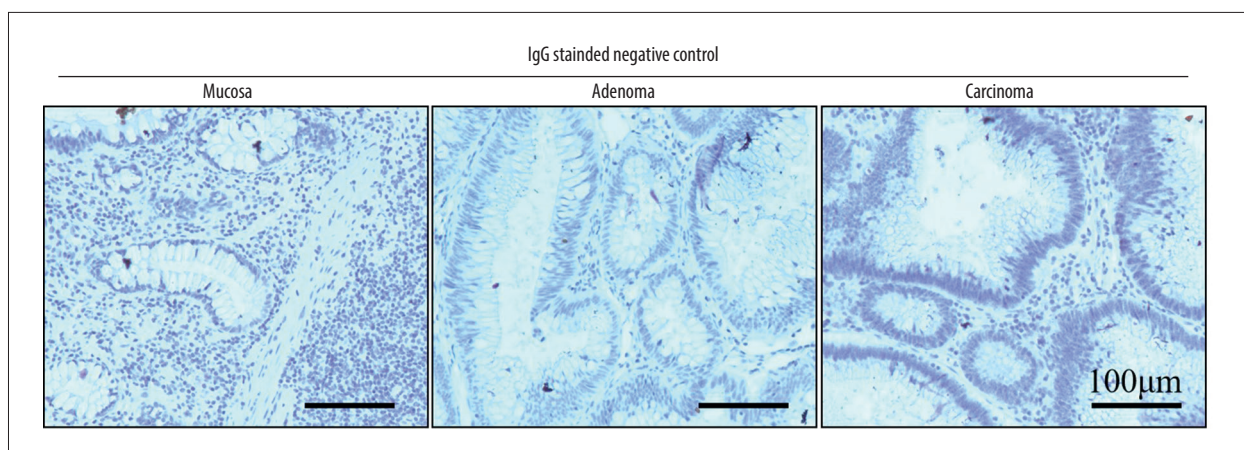
Supplementary Figure 1. The immunohistochemistry images of negative control paraffin-embedded sections stained by rabbit IgG.
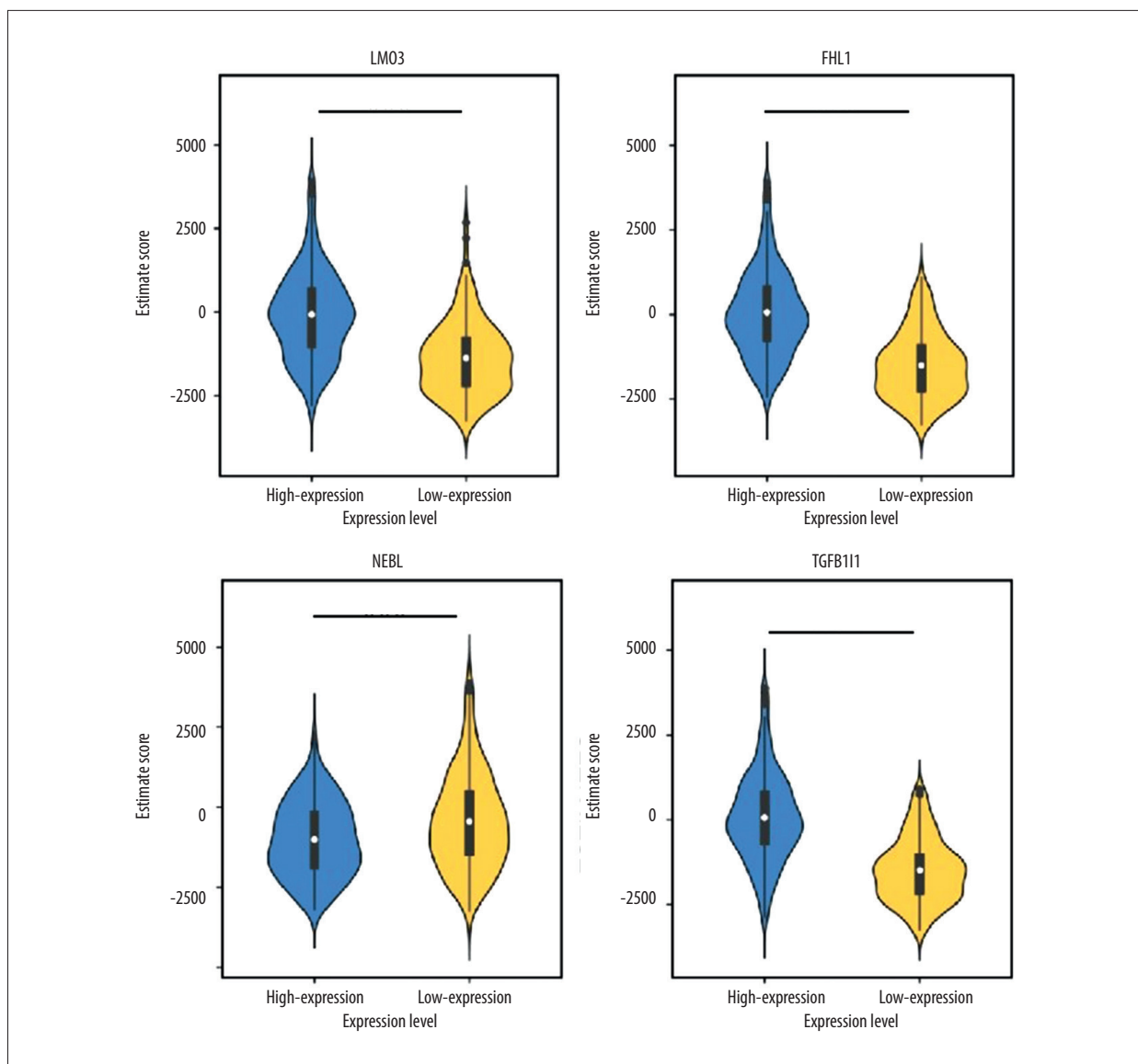
Supplementary Figure 2. The correlations of EstimateScores with expression levels of LMO3, FHL1, NEBL, and TGFB1I1. *** $P<0.001$, two-tailed unpaired t test (R, version 3.5.1).

Supplementary Figure 3. LMO3 was successfully overexpressed in HCoEpiC, HCT116, and RKO cells. The overexpressions of LMO3 in HCoEpiC, HCT116, and RKO cells were validated by SDS – PAGE at 48 h after transfection of pcDNA3.4-LMO3-3×Flag or empty vector (GraphPad, version 8.0.2).

References:

1. Yasuoka Y, Taira M. LIM homeodomain proteins and associated partners: Then and now. Curr Top Dev Biol. 2021;145:113-66

2. Sala S, Ampe C. An emerging link between LIM domain proteins and nuclear receptors. Cell Mol Life Sci. 2018;75:1959-71

3. John E, Laskow TC, Buchser WJ, et al. Zinc in innate and adaptive tumor immunity. J Transl Med. 2010;8:1-16

4. Wei X, Zhang H. Four and a half LIM domains protein 1 can be as a double-edged sword in cancer progression. Cancer Biol Med. 2020;17:270-81

5. Matthews JM, Lester K, Joseph S, Curtis DJ. LIM-domain-only proteins in cancer. Nat Rev Cancer. 2013;13:111-22

6. Ngan E, Stoletov K, Smith HW, et al. LPP is a Src substrate required for invadopodia formation and efficient breast cancer lung metastasis. Nat Commun. 2017;8:15059

7. Zhang B, Song L, Cai J, et al. The LIM protein Ajuba/SP1 complex forms a feed forward loop to induce SP1 target genes and promote pancreatic cancer cell proliferation. J Exp Clin Cancer Res. 2019;38:205

8. Bukhari S, Tandiary MA, Al-Sanea MM, et al. Small molecules as LIM kinase inhibitors. Curr Med Chem. 2021;29(17):2995-3027

9. Manetti F. Recent advances in the rational design and development of LIM kinase inhibitors are not enough to enter clinical trials. Eur J Med Chem. 2018;155:445-58

10. Guo ZS, Qu Z. PDLIM2: Signaling pathways and functions in cancer suppression and host immunity. Biochim Biophys Acta Rev Cancer. 2021;1876:188630

11. Lu G, Zhou Y, Zhang C, Zhang Y. Upregulation of LIMK1 is correlated with poor prognosis and immune infiltrates in lung adenocarcinoma. Front Genet. 2021;12:671585

12. Wu Z, Zou X, Xu Y, et al. Ajuba transactivates N-cadherin expression in colorectal cancer cells through interaction with Twist. J Cell Mol Med. 2021;25:8006-14

13. Zhang J, Guo M, Zhang J, et al. Four and a half LIM domain protein 1 as a novel prognostic biomarker and correlation with immune infiltration levels in lung adenocarcinoma. 2022

14. Keum N, Giovannucci E. Global burden of colorectal cancer: Emerging trends, risk factors and prevention strategies. Nat Rev Gastro Hepat. 2019;16:713-32

15. Smit WL, Spaan CN, Johannes DBR, et al. Driver mutations of the adenoma-carcinoma sequence govern the intestinal epithelial global translational capacity. Proc Natl Acad Sci. 2020;117:25560-70

16. Ogino S, Nosho K, Irahara N, et al. A cohort study of cyclin D1 expression and prognosis in 602 colon cancer cases. Clin Cancer Res. 2009;15:4431-38

17. de Lau W, Barker N, Clevers H. WNT signaling in the normal intestine and colorectal cancer. Front Biosci. 2007;12:471-91

18. Juanes MA. Cytoskeletal control and wnt signaling – APC's dual contributions in stem cell division and colorectal cancer. Cancers. 2020;12:3811

19. Feng M, Dong N, Zhou X, et al. Myosin light chain 9 promotes the proliferation, invasion, migration and angiogenesis of colorectal cancer cells by binding to Yes-associated protein 1 and regulating Hippo signaling. Bioengineered. 2022;13:96-106

20. Buikhuisen JY, Gomez Barila PM, Torang A, et al. AKT3 expression in mesenchymal colorectal cancer cells drives growth and is associated with epithelial-mesenchymal transition. Cancers. 2021;13:801

21. Madden SK, de Araujo AD, Gerhardt M, et al. Taking the Myc out of cancer: Toward therapeutic strategies to directly inhibit c-Myc. Mol Cancer. 2021;20:3

22. Park S, Lee C, Choi J, et al. The JAK2/STAT3/CCND2 axis promotes colorectal cancer stem cell persistence and radioresistance. J Exp Clin Canc Res. 2019;38:399

23. Herrmann AB, Müller M, Orth MF, et al. Knockout of LASP1 in CXCR4 expressing CML cells promotes cell persistence, proliferation and TKI resistance. J Cell Mol Med. 2020;24:2942-55

24. Anderson CA, Kovar DR, Gardel ML, Winkelman JD. LIM domain proteins in cell mechanobiology. Cytoskeleton. 2021;78:303-11

25. Zhang Y, An J, Pei Y. LncRNA SNHG6 promotes LMO3 expression by sponging miR-543 in glioma. Mol Cell Biochem. 2020;472:9-17

26. Xuan YW, Liao M, Zhai WL, et al. MicroRNA-381 inhibits lung adenocarcinoma cell biological progression by directly targeting LMO3 through regulation of the PI3K/Akt signaling pathway and epithelial-to-mesenchymal transition. Eur Rev Med Pharmacol. 2019;23:8411-21

27. Cheng Y, Hou T, Ping J, et al. LMO3 promotes hepatocellular carcinoma invasion, metastasis and anoikis inhibition by directly interacting with LATS1 and suppressing Hippo signaling. J Exp Clin Cancer Res. 2018;37:228

28. Aoyama M, Ozaki T, Inuzuka H, et al. LMO3 interacts with neuronal transcription factor, HEN2, and acts as an oncogene in neuroblastoma. Cancer Res. 2005;65:4587-97

29. S Q, Yin B. Mechanism of LMO3 in tumor metastasis. Int J Surg. 2019:705-8

30. Chen Y, Pei M, Li J, et al. Disruption of the CCDC43-FHL1 interaction triggers apoptosis in gastric cancer cells. Exp Cell Res. 2022;415(1):113107

31. Niu C, Liang C, Guo J, et al. Downregulation and growth inhibitory role of FHL1 in lung cancer. Int J Cancer. 2012;130:2549-56

32. Asada K, Ando T, Niwa T, et al. FHL1 on chromosome X is a single-hit gastrointestinal tumor-suppressor gene and contributes to the formation of an epigenetic field defect. Oncogene. 2013;32:2140

33. Bliss KT, Chu M, Jones-Weinert CM, Gregorio CC. Investigating lasp-2 in cell adhesion: New binding partners and roles in motility. Mol Biol Cell. 2013;24:995-1006

34. Zhang Y, Li J, Yuan Q, et al. Upregulation of LASP2 inhibits pancreatic cancer cell migration and invasion through suppressing TGF-β-induced EMT. J Cell Biochem. 2019;120:13651-57

35. Zhang Y, Zhang L. Knockdown of LASP2 inhibits the proliferation, migration, and invasion of cervical cancer cells. J Cell Biochem. 2019;120:15389-96

36. Li J, Hu S, Zhang Z, Qian L, et al. LASP2 is downregulated in human liver cancer and contributes to hepatoblastoma cell malignant phenotypes through MAPK/ERK pathway. Biomed Pharmacother. 2020;127:110154

37. Wang B, Zhang L, Zhao L, et al. LASP2 suppresses colorectal cancer progression through JNK/p38 MAPK pathway meditated epithelial-mesenchymal transition. Cell Commun Signal. 2017;15:21

38. Choi C, Finlay DK. Optimising NK cell metabolism to increase the efficacy of cancer immunotherapy. Stem Cell Res Ther. 2021;12:1-10

39. Omoto T, Kim-Kaneyama J, Lei X, et al. The impact of stromal Hic-5 on the tumorigenesis of colorectal cancer through lysyl oxidase induction and stromal remodeling. Oncogene. 2018;37:1205-19

40. Du X, Xu Q, Pan D, et al. HIC-5 in cancer-associated fibroblasts contributes to esophageal squamous cell carcinoma progression. Cell Death Dis. 2019;10:1-16

41. Winkler J, Abisoye-Ogunniyan A, Metcalf KJ, Werb Z. Concepts of extracellular matrix remodelling in tumour progression and metastasis. Nat Commun. 2020;11:1-19